Current through a combined magnetostatic and electrostatic barrier system

C. Heide
University of Oxford, Department of Physics, Theoretical Physics, 1 Keble Road, Oxford OX1 3NP, United Kingdom
(Received 4 January 1999)

A device is proposed where a gated ferromagnetic strip is placed on top of a semiconductor heterostructure to form a combined magnetostatic and electrostatic barrier. On the basis of a simple model which is of the Landauer-Büttiker type, the current-voltage characteristics are studied, and it is shown that the electron motion can be tuned between three different regimes: quasiclassical behavior, usual barrier tunneling, and resonant tunneling. [S0163-1829(99)01728-2]

I. INTRODUCTION

The Landau quantization of the electron motion by an external magnetic field can give much information about the behavior of a homogeneous two-dimensional electron gas as is particularly well demonstrated with the quantum Hall effect.[1] Further interesting diamagnetic effects occur in magnetotransport if the two-dimensional electron gas is nonhomogeneous.[2] By alternating either the magnetic field or an electric field on mesoscopic length scales, it is possible to achieve different kinds of modulations.

Recent work on nonhomogeneous two-dimensional electron systems has been based on GaAs/Al_xGa_{1-x}As heterojunctions overlaid with patterned metallic gates, ferromagnetic metals, or superconducting materials. In the case of a weak periodic one-dimensional electrostatic potential, Weiss *et al.* observed oscillations in the magnetoresistance as the external magnetic field applied perpendicularly to the electron gas is varied continuously.[3] If the potential forms an antidot array, Roukes *et al.* could show that the Hall resistivity becomes negative and quenched.[4] The effects of a modulated magnetic field acting on a two-dimensional electron gas have been reported by Carmona *et al.*[5,6] and Ye *et al.*,[7] who used either patterned superconducting or ferromagnetic gratings. The oscillations in the magnetoresistance depend characteristically on the magnetization direction of these individual micromagnets as a function of the external, i.e., homogeneous, magnetic field.

Since the oscillations in the magnetoresistance observed by Weiss *et al.* show the interesting commensurability effect of two different length scales—the period of the modulation potential and the cyclotron radius of the electrons at the Fermi energy—analogies have been sought on a theoretical level in a magnetostatical modulated two-dimensional electron gas prior to the experiments in Refs. 5–7. Müller, for example, analyzed the effects of a magnetic field that varies linearly across the electron gas, and found that the electrons can flow only in the direction perpendicular to the field gradient.[8] Different ''magnetic'' structures, such as a potential well or barrier created by a finite magnetic field, were considered by Peeters and Matulis.[9] Again the magnetostatic potential influences the transmission as the wave vector of the electron wave function shows the two-dimensional nature of the electron motion. A similar problem was investigated independently by Calvo, who pointed out that in a continuously varying magnetostatic potential the discrete and continuum energy spectra overlap so that the motion of the electron can be understood in terms of the classical cyclic, diamagnetic motion.[10] A combination of such simple magnetic structures leads to so-called magnetic superlattices which show commensurability effects as their electrostatic equivalents with the difference that now apart from the cyclotron radius of the electrons the magnetic-field modulation gives the characteristic length scale.[11] Comparing their experimental results with these calculations of Peeters and Vasilopoulos, Ye *et al.* could further show that the magnetic strip lattice leads to an additional weak strain-induced electrostatic potential modulation of the underlying electron gas.[7] The additional electrostatic potential modulation was also reported by the group of Carmona *et al.*, who could separate the different contributions to the magnetoresistance as they studied its temperature dependence above and below the transition temperature for superconductivity for the used lead or niobium grating.[5,6]

This paper proposes a structure of the opposite limit: a combination of a strong magnetostatic and electrostatic potential. The device consists of a GaAs/Al_xGa_{1-x}As semiconductor heterostructure, which forms a two-dimensional electron gas at the interface and a ferromagnetic strip placed on top with an easy axis of magnetization perpendicular to the underlying electron gas as shown in Fig. 1. In addition, the strip is gated to form a combined magnetostatic and electrostatic barrier for the conduction electrons. On the basis of a simple model, such a structure is shown to have three different regimes of operation. Whereas for a certain regime electrons can move according to the classical diamagnetic motion, there is also the possibility to tune the device between resonant and nonresonant tunneling behavior. This property could be exploited in magnetic and magneto-optic devices to be used as digital logic circuits.

In order to calculate the current-voltage characteristics of the proposed structure, it is built on a slight modification of the nonequilibrium coupling formalism developed by Caroli *et al.*[12] and Feuchtwang.[13] This leads to a simple extension of the Landauer-Büttiker formula[1] including now the effects of the two-dimensional electron motion. Somewhat related to this subject is the work of Guéret *et al.*[14] and Ramaglia *et al.*,[15] who investigated the effect of a transverse magnetic field on the tunnel current through thick and low semiconductor barriers.

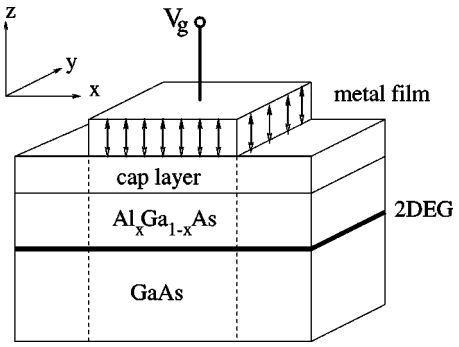

FIG. 1. Schematic cross section of a semiconductor heterostructure segment with a gated ferromagnetic metal layer on top that modulates the underlaying two-dimensional electron gas (2DEG) to form a combined magnetostatic and electrostatic barrier potential. In particular, the ferromagnet has an easy axis perpendicular to the electron gas, so that the magnetic field is directed either along the positive or negative z direction, and the gate voltage V_g controls the depletion of the electron gas.

The remainder of the paper is structured as follows. In Sec. II the model of a combined magnetostatic and electrostatic barrier system is introduced. Then in Sec. III, the Landauer-type formula is derived for the essentially two-dimensional electron motion. A numerical example is studied in Sec. IV to show that tunneling through a combined magnetostatic and electrostatic barrier can be tuned between resonant and nonresonant tunneling. In conclusion the results are discussed and summarized in Sec. V.

II. MODEL OF A COMBINED MAGNETOSTATIC AND ELECTROSTATIC BARRIER SYSTEM

In the following, a model description is given of the proposed structure shown in Fig. 1. The interface between GaAs and $Al_xGa_{1-x}As$ is approximated in Fig. 2 by an infinite two-dimensional electron gas occupying the xy plane in a three-dimensional space. The overlying ferromagnetic metal strip is gated and creates ideally a square potential barrier of the height V_0 in the xy plane extending from $\mathcal{L}=-a$ to $\mathcal{R}=a$ in the x direction. Further, the magnetization of the ferromagnet is perpendicular to the two-dimensional electron gas so that the magnetic field $\mathbf{B}$ is in the perpendicular z direction on the same finite strip as the electrostatic potential,

$$B_z(x)=B\,\Theta(x-\mathcal{L})\Theta(\mathcal{R}-x), \tag{1}$$

where $B=-|B|$ is the uniform strength of the field. A similar model has been used to approximate the tunneling through thick barrier diodes under the influence of a magnetic field, where it is assumed that for very thick barriers the broadening of the Landau levels on both sides is significant enough to view them as a continuum of incoming and outgoing states.[14] Contrary to other popular two-dimensional electron-gas systems, such as a Hall bar, the proposed model is not confined along the x direction. This yields a considerable mathematical simplification and emphasizes tunneling rather than transport along the edges of the system. Since the field is applied within a finite strip, the system naturally separates into the leads on the left and right side of the potential barrier in the intermediate region so that the Hamiltonian of the system is a sum of three independent parts,

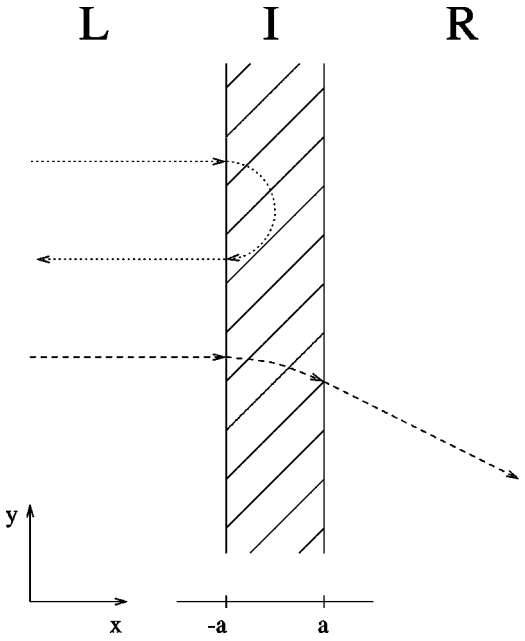

FIG. 2. Two perfectly conducting leads L and R are connected to different external reservoirs. They have partitions $\mathcal{L}=-a$ and $\mathcal{R}=a$, respectively, with the combined magnetostatic and electrostatic barrier potential in the intermediate region I.

$$H=\Theta(\mathcal{L}-x)H_L+\Theta(x-\mathcal{L})\Theta(\mathcal{R}-x)H_I+\Theta(x-\mathcal{R})H_R. \tag{2}$$

With this form of the Hamiltonian it is possible to derive a quantum-statistical formulation based on Green's functions rather than matching up wave functions as was shown by Caroli *et al.* and Feuchtwang.[12,13] The Green's functions of the three uncoupled subspaces, L, I, and R, are then determined by

$$[\hbar\omega-H_p]g_p(\mathbf{r},\mathbf{r}';\omega)=\delta(\mathbf{r}-\mathbf{r}'), \tag{3}$$

with $\mathbf{r},\mathbf{r}'$ defined in the respective subregion $p\in\{L,I,R\}$. The Green's function G of the full system has an analogous definition.

In order to connect the uncoupled regions of the system or in other words to couple the Green's functions g_p to find G, one has to be aware of the fact that in a quantum-mechanical formulation the vector potential $\mathbf{A}$ is the fundamental physical field rather than the magnetic field $\mathbf{B}$, and that the vector potential can be nonvanishing while at the same time the magnetic field is zero. Since the system (Fig. 2) is invariant along the y direction, a generalized Landau gauge $A_y=Bx+\text{const}$ is independent of the y coordinate. Furthermore, the vector potential is required to be continuous across the partitions, which in conjunction with Eq. (1) determines $\mathbf{A}$ as

$$A_x(x,y,z)=0,$$

$$A_y(x,y,z)=\begin{cases} B\,\mathcal{L} & \text{if} \quad x\leqslant\mathcal{L} \\ Bx & \text{if} \quad \mathcal{L}\leqslant x\leqslant\mathcal{R} \\ B\,\mathcal{R} & \text{if} \quad \mathcal{R}\leqslant x, \end{cases} \tag{4}$$

$$A_z(x,y,z)=0.$$

The effect of the magnetic field on the conduction electron spin is small in typical heterostructures such as GaAs/$Al_xGa_{1-x}As$ so that it is neglected here.

Even without the magnetic field, the band structure is discontinuous at the interfaces $\mathcal{L},R$ and the potential changes by the amount V_0. In equilibrium the barrier is considered to be flat on top, while upon biasing the junction the potential of the barrier acquires a slope and the chemical potential μ^R in the right lead undergoes a shift eV with respect to the chemical potential μ^L in the left lead. Simultaneously, the conduction-band bottom V_0^R in the right lead shifts by eV with respect to the conduction-band bottom V_0^L in the left lead. The corresponding single-particle potential acquires the form

$$V_0(x)=\left[V_0-eV\frac{x-\mathcal{L}}{\mathcal{R}-L}\right]\Theta(x-\mathcal{L})\Theta(\mathcal{R}-x)-eV\Theta(x-\mathcal{R}). \tag{5}$$

Here, e is the modulus of the elementary charge of the electron and V is the voltage drop across the barrier. This leads to the following model Hamiltonians of the subsystems:

$$H_I=\frac{1}{2m}\left(\mathbf{p}+\frac{e}{c}\mathbf{A}_I\right)^2+V_0(x), \tag{6}$$

$$H_p=\frac{1}{2m}\left(\mathbf{p}+\frac{e}{c}\mathbf{A}_p\right)^2, \tag{7}$$

where $p\in\{L,R\}$. The vector potential in the corresponding subspace is now denoted by $\mathbf{A}_p$; $\mathbf{p}=-i/\hbar\nabla$ is the canonical momentum. Choosing the gauge (4), the Hamiltonian H_I of the intermediate region (6) transforms into

$$H_I=-\frac{\hbar\omega_c}{2}\left[a_B^2\Delta-2ix\partial_y-\left(\frac{x}{a_B}\right)^2-\frac{2}{\hbar\omega_c}V_0(x)\right], \tag{8}$$

where the expression inside the square brackets is dimensionless with the magnetic length $a_B=\sqrt{\hbar/(m\omega_c)}$, the cyclotron frequency $\omega_c=|eB|/(mc)$, the effective mass m, and the two-dimensional Laplace operator Δ. By using this particular gauge, the electron wave function separates into a product of functions for the individual coordinates and the mathematical model becomes translational invariant in the y direction. Therefore, all the Green's functions can also be Fourier transformed in the y coordinate,

$$g_p(x,y,x',y';\omega)=\int_{-\infty}^{\infty}\frac{dk_y}{2\pi}e^{ik_y(y-y')}g_p(x,x';k_y;\omega), \tag{9}$$

where g_p with $p\in\{L,I,R\}$ is a Green's function of the subparts and k_y is the electron wave vector in the y direction. According to Eq. (3), the Green's function of the intermediate region g_I fulfills the inhomogeneous differential equation,

$$\frac{\hbar\omega_c}{2}\left[a_B^2\partial_x^2-\left(\frac{x-x_0}{a_B}\right)^2+2\nu+1\right]g_I(x,x';k_y;\omega)=\delta(x-x'), \tag{10}$$

where the following parameters were introduced for convenience:

$$\nu=\frac{1}{\hbar\omega_c}\left(\hbar\omega-V_0-eV\frac{\mathcal{L}-a_B^2k_y}{\mathcal{R}-L}\right)+\left(\frac{eV}{\hbar\omega_c}\frac{a_B}{\sqrt{2}(\mathcal{R}-L)}\right)^2-\frac{1}{2}, \tag{11}$$

$$x_0=a_B^2\left(k_y+\frac{eV}{\hbar\omega_c}\frac{1}{\mathcal{R}-L}\right). \tag{12}$$

The solution of the homogeneous form of the differential equation (10) $\nu_{1,2}$ is known in forms of parabolic cylinder functions (see the Appendix) $\nu_1=D_\nu[(x-x_0)\sqrt{2}/a_B]$ and $\nu_2=D_\nu[(x_0-x)\sqrt{2}/a_B]$ so that with the help of Eq. (9) (Ref. 16) the Green's function of the intermediate region g_I can be constructed. Since in the leads the conduction electrons travel freely and obey the dispersion law $\epsilon^{L(R)}=\hbar^2q_{L(R)}^2/(2m)$, the corresponding Green's functions are those of free waves.[1] The electron wave vectors include a contribution from the nonvanishing vector potential, i.e., in the left lead $q_L=\sqrt{2m\,\omega/\hbar-(\mathcal{L}/a_B^2-k_y)^2}$ whereas in the right lead the shift due to the bias needs to be included, $q_R=\sqrt{2m(\hbar\omega+eV)/\hbar^2-(\mathcal{R}/a_B^2-k_y)^2}$.

In order to gain a better intuitive understanding of the system, it is useful to discuss the classical analogy. Classically, electrons move when they are confined entirely within the barrier strip on Larmor circles with radius $r_c=\sqrt{2E/(m\omega_c^2)}$, where E is the classical energy of the electron. It is assumed for a moment that $V_0=0$ and that an electron coming from an area outside the barrier, say L as in Fig. 2, is scattered by the magnetic strip I. There are two conceivable ways in which the electron can be scattered. In the first case, shown in the upper part of Fig. 2, if the momentum of the electron in the x direction is so low that its associated cyclotron radius r_c is smaller than half the width of I, the electron is reflected back into the region from where it is incident. In the second case, shown in the lower part of Fig. 2, if the momentum in the x direction is high enough so that its cyclotron radius r_c is larger than half the width of I, the electron can overcome the threshold imposed by the magnetic field and is scattered into the region R. If the present situation is described by quantum mechanics, the problem is somewhat analogous to that of electron reflection at a potential step in the case of low momentum in the x direction of the incident conduction electron and to that of electron transmission above a potential well for the high momentum case. Thus, this result leads to an electron motion that varies only slightly from the classical case.[9] The effect of the magnetostatic barrier is that of a momentum filter.

If an additional electrostatic barrier is included, $V_0>0$, the system shows in a classical picture no substantial difference from the previous case. Quantum mechanically one would, on the other hand, expect that due to the combined electrostatic and magnetostatic potentials quasibound states in the barrier region I can form and can give rise to a resonant behavior in the transmission. For the same reasons as given in the example earlier, it is possible to observe the latter effect only for electron energies that exceed the barrier

height of the magnetostatic potential. If, however, the energies and momenta of certain electrons correspond to the quasibound states in the barrier region *I*, these electrons can tunnel into the quasibound states and their transmission through the barrier becomes strongly pronounced. The barrier acts then as a momentum and energy filter. Therefore, it should be interesting to analyze the current-voltage behavior for such a system in order to test if this quasi-resonant tunneling leads to a current-voltage characteristic that shows negative resistance.

III. CURRENT

The formulations by Landauer and Büttiker for currents through a finite region of noninteracting electrons have contributed significantly to the clear understanding of mesoscopic transport as long as it is coherent across the device. In this section, it is shown that the two-dimensional motion of the electron through the combined magnetostatic and electrostatic barrier can also be understood within the framework of the Landauer-Büttiker formalism.

In the present case the conduction current operator can be written as a sum of the volume density of the charge flux and the diamagnetic contribution $\mathcal{I}=\mathcal{I}^{\mathrm{vd}}+\mathcal{I}^{\mathrm{dia}}$, where the individual terms expressed through field operators in the notation of second quantization read as

$$\mathcal{I}^{\mathrm{vd}}=\frac{ie\hbar}{2m}[(\nabla\Psi^{\dagger})\Psi-\Psi^{\dagger}(\nabla\Psi)], \tag{13a}$$

$$\mathcal{I}^{\mathrm{dia}}=-\frac{e^2}{mc}\Psi^{\dagger}\mathbf{A}\Psi. \tag{13b}$$

Since the system is assumed to be in steady state and translationally invariant along the *y* direction, the current can be Fourier transformed with respect to these quantities. Further, only conduction electrons that cross the barrier are considered so that the current due to the contributions (13) yields when taking the average

$$\langle\mathcal{I}\rangle=\sum_{\alpha\beta}\int_{-\infty}^{\infty}\frac{dk_y}{2\pi}\int_{-\infty}^{\infty}\frac{d\omega}{2\pi}\lim_{x'\to x}\left[\frac{e\hbar}{2m}(\partial_{x'}-\partial_x)+\frac{ie^2}{mc}A_x\right]\times G^{<}(x,x';k_y;\omega), \tag{14}$$

where the average over the field operators is written in terms of the Keldysh Green's function $G^{<}(x,x';k_y;\omega)=i\langle\Psi^{\dagger}(x';k_y;\omega)\Psi(x;k_y;\omega)\rangle$. The current (14) may be calculated at any point in the system, for example at one of the partitions $\mathcal{P}\in\{\mathcal{L},R\}$, since in a steady state the continuity equation $\nabla\langle\mathcal{I}\rangle=0$ holds.

A further significant simplification is obtained by the form of the gauge in Eq. (4). As $A_x=0$, the magnetic-field dependence of Eq. (14) is only contained implicitly through k_y. Therefore the current (14) takes the same form as in usual electrostatic barrier tunneling of noninteracting electrons. Meir and Wingreen have shown that in such a case the usual two-terminal Landauer formula is retained.[17] Employing this result, the current is given by

$$\langle\mathcal{I}\rangle=-2e\int_{-\infty}^{\infty}\frac{d\omega}{2\pi}[n_F^L(\omega)-n_F^R(\omega)]\int_{-\infty}^{\infty}\frac{dk_y}{2\pi}T(k_y,\omega), \tag{15}$$

and differs from the Landauer formula only in that the transmission coefficient through the intermediate region

$$T(k_y,\omega)=\hbar^2\,G^a(\mathcal{L},R;k_y;\omega)G^r(\mathcal{R},L;k_y;\omega)\times v_L(k_y;\omega)v_R(k_y;\omega)$$

depends explicitly on k_y. The quantities $v_p(k_y;\omega)=\hbar q_p/m$ are the electron velocities in the leads. Since the Green's functions of the subregions are known, the full Green's function $G^{(r/a)}$ can be obtained according to the coupling formalism of Caroli and Feuchtwang.[12,13] The transmission coefficient then takes the form

$$T(k_y,\omega)=\frac{4W^2q_Lq_R}{(\Omega+q_Lq_R\Lambda)^2+(q_L\Gamma_R+q_R\Gamma_L)^2}, \tag{16}$$

where the following notations have been introduced (see also Ref. 16):

$$\Gamma_p=[v_1'(x)v_2(\mathcal{R})-v_2'(x)v_1(\mathcal{R})]_{x=\mathcal{P}}, \tag{17a}$$

$$\Omega=[v_1'(x)v_2'(x')-v_2'(x)v_1'(x')]_{x=\mathcal{L},x'=\mathcal{R}}, \tag{17b}$$

$$\Lambda=v_1(\mathcal{L})v_2(\mathcal{R})-v_2(\mathcal{L})v_1(\mathcal{R}), \tag{17c}$$

and W is the Wronskian (see the Appendix). The prime indicates the derivative of the parabolic cylinder functions $v_{1,2}(x)$ with respect to their argument x. Equation (15) shall now be used to analyze the current-voltage characteristics of the combined magnetostatic and electrostatic barrier potential.

IV. NUMERICAL RESULTS AND DISCUSSION

In this section, Eq. (15) is evaluated numerically as a function of the applied bias at zero temperature. In order to obtain a better estimate of the physical quantities involved, an explicit model of the GaAs/Al_xGa_{1-x}As semiconductor heterostructure with a ferromagnetic strip placed on top as introduced in Fig. 1 is considered. According to Crowell *et al.*,[18] it is possible to grow ferromagnetic films on semiconductor heterostructures where the magnetic field inside the structure can approximately be up to $B=5$ kG. Here, it is assumed that the field felt by the two-dimensional electron gas will be $B=1$ kG. The magnetic length a_B is then approximately 80 nm so that the barrier width of $s=6.0a_B/\sqrt{2}$, used in the numerical example, corresponds to roughly 350 nm. An effective mass of $m=0.07\,m_e$ and an electron density of $n_s=5\times10^{11}/\mathrm{cm}^2$ for GaAs lead to a Fermi energy $E_F=16.5$ meV or $E_F/(\hbar\omega_c)\approx1$.

Figure 3 shows the current $C(V_n)=-\langle\mathcal{I}\rangle/2$ as a function of the normalized voltage $V_n[eV/\hbar\omega_c]$. The barrier in Fig. 3 has a width of $s=6.0a_B/\sqrt{2}$ and a height at zero magnetic field and zero bias of $U=1.50$, $U=1.75$, $U=2.00$, and $U=2.25$ for the different plots, respectively, where $U=V_0/E_F$. The fact that no current flows for voltages below 3×16.5 mV $=49.5$ mV is due to a threshold of the combined barrier system and shall be discussed in detail below.

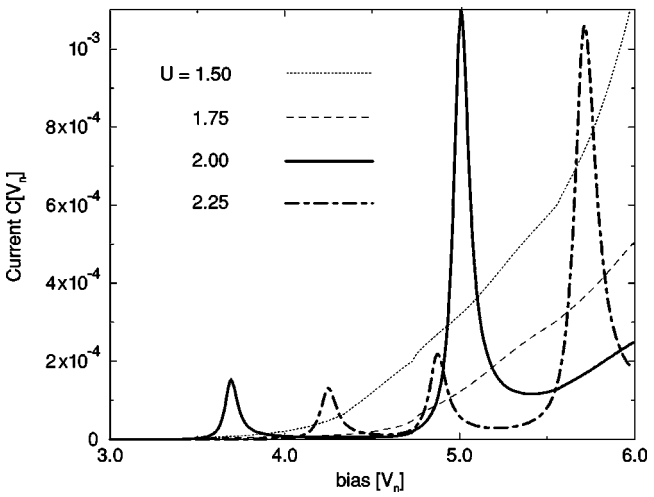

FIG. 3. Current-voltage characteristics for barrier width of $s=6.0a_B/\sqrt{2}$ and different potential heights $U=V_0/E_F$. The current $C(V_n)=-\langle\mathcal{I}\rangle/2$ is given as a function of the normalized voltage $V_n[eV/\hbar\omega_c]$.

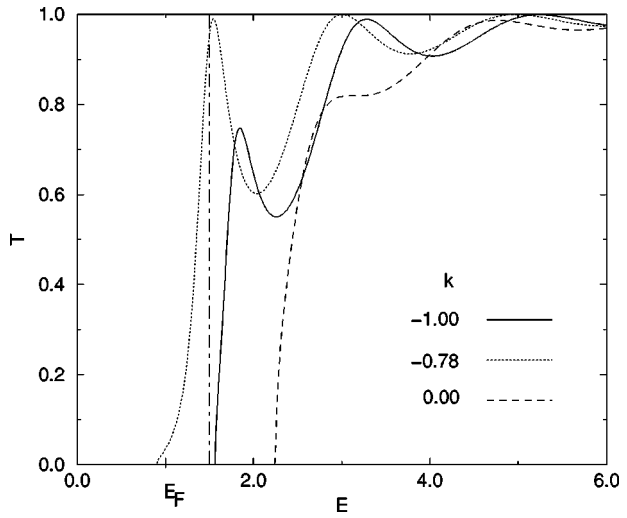

FIG. 4. Transmission coefficients as a function of $E=\hbar\omega/(\hbar\omega_c)$ for different $k=a_Bk_y$ through a barrier with width $s=6.0a_B/\sqrt{2}$, height $U=1.50$ depicted by the dash-dotted line, and applied bias of 58 mV.

The current-voltage characteristics for $U=1.50$ and $U=1.75$ show more or less typical single barrier tunneling behavior in the voltage range calculated. For $U=2.00$ and $U=2.25$, however, the functions plotted in Fig. 3 behave very differently. In particular, for $U=2.00$ peaks occur in the current-voltage characteristic at 61 mV and 82 mV, whereas for $U=2.25$ at 70 mV, 79 mV, and 95 mV, respectively. This kind of behavior is similar to resonant tunneling through a double-barrier structure.

In the following it shall be explained how the three different regimes in the structure occur. The existence of a threshold voltage $V_{\rm th}$ can be deduced from the nonvanishing vector potential $\mathbf{A}$ in the leads which complicates the wave-vector dependence of the current in the direction parallel to the interfaces, expressed by k_y. In order for a current to flow, both wave vectors in the leads q_L and q_R have to be real so that an electron can propagate from the left to the right side of the barrier. This leads to the requirement for the wave vectors to be real,

$$\frac{E_F}{\hbar\omega_c}\geqslant\frac{1}{2}(\mathcal{L}-a_B^2k_y)^2, \tag{18}$$

$$\frac{1}{\hbar\omega_c}(E_F+eV)\geqslant\frac{1}{2}(\mathcal{R}-a_B^2k_y)^2. \tag{19}$$

Using Eq. (18) to obtain a condition for k_y and inserting the result into Eq. (19), one finds a threshold voltage above which a current starts to flow,[15]

$$\frac{eV_{\rm th}}{\hbar\omega_c}=\frac{1}{2}(\mathcal{R}-L)^2-\sqrt{\frac{2E_F}{\hbar\omega_c}}(\mathcal{R}-L). \tag{20}$$

In the numerical example $V_{\rm th}$ is 49.5 mV.

Next the wave-vector dependence of the transmission coefficient $T(k_y)$ shall be discussed in the regime where tunneling is comparable to single barrier tunneling. In Fig. 4 the transmission coefficient is shown for $k=0.00$, $k=-0.78$, and $k=-1.00$ at an applied bias of 58 mV, where $k=a_Bk_y$. Only for the second value $k=-0.78$ does the transmission coefficient have a finite value below the Fermi energy E_F. In this range, it is a monotonic function of the energy and is tantamount to the transmission coefficient for typical single-barrier tunneling. In order to see why this frequency cutoff occurs, the corresponding one-dimensional barrier potential is depicted in Fig. 5. In the graph for $k=0.00$, only the right lead can have propagative states, i.e., only q_R is real, and in the graph for $k=-1.00$ only the left lead can, i.e., only q_L is real, whereas for $k=-0.78$ both q_L and q_R are real such that tunneling through the barrier is made possible between allowed states. Nevertheless, there is no apparent configuration where an energy level of the well coincides with a propagative state outside the barrier.

Finally, to understand the resonant behavior of the current-voltage characteristic in Fig. 3 for $U=2.00$ and $U=2.25$, one has to turn again to the wave-vector-dependent transmission coefficient $T(k_y)$. Similar to before, in Fig. 6 the transmission coefficient for $U=2.00$ is shown for $k=0.00$, $k=-0.78$, and $k=-1.00$ at an applied bias of 58 mV. Again only for the second value $k=-0.78$ is there transmission at the Fermi energy E_F. This time the transmission coefficient, however, shows a sharp peak. The peak does not quite reach unity due to the asymmetry in the potential as illustrated for $k=-0.78$ in Fig. 7. Further, one can see that the Fermi energy in the lead corresponds to a state at ap-

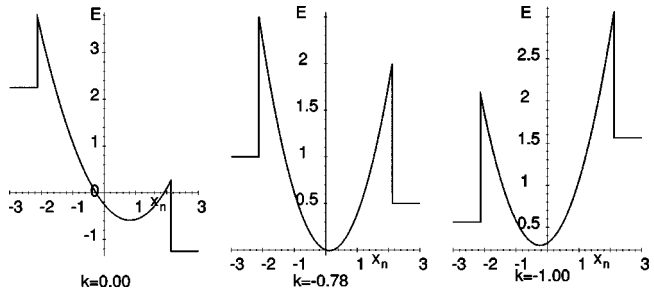

FIG. 5. One-dimensional barrier potential for different values of $k=a_Bk_y$ corresponding to Fig. 4. The abscissa is given in terms of $x_n=x/a_B$ and the ordinate of $E=\hbar\omega/(\hbar\omega_c)$.

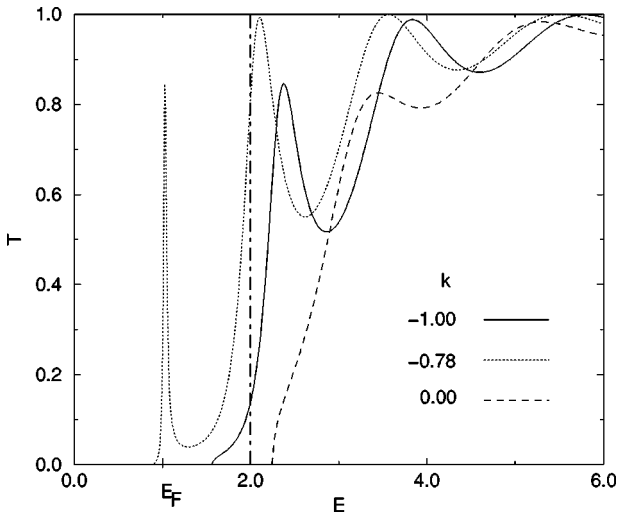

FIG. 6. Transmission coefficients as a function of $E=\hbar\omega/(\hbar\omega_c)$ for different $k=a_B k_y$ through a barrier with width $s=6.0a_B/\sqrt{2}$, height $U=2.00$ depicted by the dash-dotted line, and applied bias of 58 mV.

proximately $\hbar\omega_c/2$ in the barrier well measured from the bottom of the well. In a free-electron gas subjected to a homogeneous magnetic field, $\hbar\omega_c/2$ would be the energy of the first Landau level. Thus the peak in the transmission through the barrier is created by tunneling through a quasibound state of the barrier well.

This leads to the following interpretation of the current-voltage characteristics in the cases for $U=2.00$ and $U=2.25$. Below the threshold voltage V_{th} no current can flow since there is no transmission through the barrier. Above V_{th} tunneling through the structure is still reduced, because the tunneling length must extend over the entire width of the barrier as is the case for single-barrier tunneling. When the bias is further increased, the well formed by the magnetic field is pulled down to lower energies until the well level becomes degenerate with the Fermi energy for certain k_y values of the conduction electrons incident from the left lead. This leads to resonant tunneling through the quasibound state of the well. Increasing the bias even further, so that the well level drops sufficiently below the Fermi level but not necessarily below the conduction-band edge, the current flow is strongly reduced again, leading to a negative differential conductivity. Although the k_y-wave-vector dependence in the quasi-one-dimensional potential leads to a cutoff in the integration in Eq. (15), it does not shift the energy levels in the barrier well and therefore the resonances do not become significantly smeared out in the current-voltage characteristics. The effect of this wave-vector-dependent tunneling is that the current-voltage characteristics very much attain a one-dimensional character, i.e., most of the tunneling occurs in a narrow region of k_y and close to the Fermi level of the left lead. Therefore, the current is reduced when the bias is increased after crossing a resonance level before a new one is encountered.

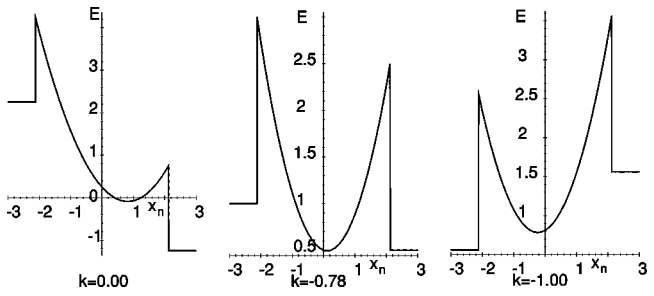

FIG. 7. One-dimensional barrier potential for different values of $k=a_B k_y$ corresponding to Fig. 6. The abscissa is given in terms of $x_n=x/a_B$ and the ordinate of $E=\hbar\omega/(\hbar\omega_c)$.

V. CONCLUSION

A current or conductance measurement on devices where transport is ballistic usually faces problems when dealing with a strong bias where the system cannot be assumed to be near equilibrium. In the present case this situation is complicated by the presence of an inhomogeneous magnetic field. To date, both problems have been overcome only by a quasiequilibrium approximation[19] or other phenomenological approaches such as a combination of the Boltzmann and Schrödinger equation[20] or the transfer Hamiltonian formalism.[2] In Sec. III an explicit formula for the current of a two-dimensional electron gas in a nonhomogeneous external magnetic field was derived from first principles on the basis of the nonequilibrium coupling theories of Caroli *et al.* and Feuchtwang.[12,13] However, it turned out that Eq. (15) is tantamount to the usual two-terminal Landauer formula and thus illustrates well the universal character of Landauer's scattering approach to transport in the ballistic regime.

Further, in Sec. IV numerical results of the current-voltage characteristics were obtained and showed that the electrons can in fact tunnel resonantly through a combined electrostatic and magnetostatic barrier potential in a two-dimensional electron gas. Although it is possible to transform the problem such that its mathematical formulation becomes one-dimensional, the tunneling probability still depends on the electron wave vector k_y, i.e., on the momentum parallel to the barrier. The motion is essentially two-dimensional as would be expected from the classical analogy. Studying the current-voltage behavior, three regimes were found. The first, for biases below the threshold voltage V_{th}, corresponds to the classical reflection of electrons from the barrier. The other two regimes, which arise at biases above V_{th}, can only be understood on a quantum level. Depending on the ratio between electrostatic barrier height V_0 and Fermi energy in the left lead E_F, either resonant or nonresonant tunneling occurs. Further, due to the narrow range of possible values for the wave vector k_y to show resonant tunneling behavior, the motion of the conduction electrons becomes essentially one-dimensional in this regime and the combined barrier acts as a momentum and energy filter.

The fact that the tunneling behavior is tunable as a function of the electrostatic barrier height V_0 and dependent on the magnetic field B makes the proposed structure an interesting candidate for future applications in digital logic circuits. However, to make reliable predictions on the device performance, it is necessary to take into account, for example, the edge effects of the magnetic field[18] and the stress of the ferromagnetic film on the two-dimensional electron gas.[21] Further, inelastic-scattering effects are of importance

in a realistic description of transport, as has been shown for double-barrier tunneling by Wingreen *et al.*[22] It is questionable in the case of electron-phonon scattering whether or not sidebands would blur the transmission to a degree where resonances would no longer fade out before a new one occurs so that the effect of negative resistance would be suppressed.

ACKNOWLEDGMENTS

I would like to thank Dr. N. F. Johnson, Dr. P. C. Klipstein, Dr. N. F. Schwabe, and Dr. G. Bruun for making useful suggestions.

APPENDIX: PARABOLIC CYLINDER FUNCTIONS

The parabolic cylinder functions are defined in the following through Kummers's functions:[23]

$$D_\nu(\xi\sqrt{2})=2^{\nu/2}e^{-\xi^2/2}\left[\frac{\Gamma\left(\frac{1}{2}\right)}{\Gamma\left(\frac{1-\nu}{2}\right)}\Phi\left(-\frac{\nu}{2},\frac{1}{2},\xi^2\right)+\frac{\Gamma\left(-\frac{1}{2}\right)}{\Gamma\left(-\frac{\nu}{2}\right)}\xi\,\Phi\left(\frac{1-\nu}{2},\frac{3}{2},\xi^2\right)\right], \tag{A1}$$

where

$$\Phi(a,c,z)=\frac{\Gamma(c)}{\Gamma(a)}\sum_{n=0}^{\infty}\frac{\Gamma(a+n)}{\Gamma(c+n)}\frac{z^n}{n!}. \tag{A2}$$

Both $\Phi(-\nu/2,1/2,\xi^2)$, and $\xi\,\Phi(1-\nu/2,3/2,\xi^2)$ are linearly independent solutions of Kummer's differential equation in the neighborhood of $z=0$ with $z\equiv\xi\sqrt{2}$ and thus represent a series expansion for the parabolic cylinder functions around $z=0$. The functions $D_\nu(z)$ and $D_\nu(-z)$ are not the only set of possible independent solutions to the harmonic-oscillator differential equation. As can be seen from the differential equation, $D_{-\nu-1}(iz)$ and $D_{-\nu-1}(-iz)$ can also form a set of linear independent solutions from which any two combinations are essentially connected via a linear relation,[23]

$$D_\nu(z)=e^{i\pi\nu}D_\nu(-z)+\frac{\sqrt{2\pi}}{\Gamma(-\nu)}e^{i(\pi/2)(\nu+1)}D_{-\nu-1}(-iz). \tag{A3}$$

It is now possible to represent the parabolic cylinder functions for noninteger values of ν by an asymptotic expansion in terms of a power series in $1/z$ in the neighborhood of $z=\infty$. However, the asymptotic expansion for $D_\nu(z)$ will change drastically in its behavior if the argument changes sign. In other words, a phase change in the argument leads to a discontinuity at certain phase angles which results from the fact that asymptotic series are not unique. Therefore, one has to take care of the range of the argument under which the function has a certain series expansion, and one finds for phase angles $|\phi|<3/4\pi$, where $z=|z|\exp(i\phi)$, the following asymptotic expansion:

$$D_\nu(z)\approx e^{-(1/4)z^2}z^\nu\left(1-\frac{\nu(\nu-1)}{2z^2}+\frac{\nu(\nu-1)(\nu-2)(\nu-3)}{8z^4}-\cdots\right). \tag{A4}$$

To obtain now the asymptotic form for values of ϕ not comprised in the above range, one uses the linear relation (A3) in order to be able to assign values to the phase of z in a different range, e.g., $5/4\pi>\phi>1/4\pi$. Since the phase of $-z$ and $-iz$ is now $\phi-\pi$ and $\phi-1/2\pi$, this leads to

$$\begin{aligned}D_\nu(z)\approx{}& e^{-(1/4)z^2}z^\nu\left(1-\frac{\nu(\nu-1)}{2z^2}+\frac{\nu(\nu-1)(\nu-2)(\nu-3)}{8z^4}-\cdots\right)\\&+\frac{\sqrt{2\pi}}{\Gamma(-\nu)}e^{i\pi(\nu+1)}e^{(1/4)z^2}z^{-\nu-1}\left(1+\frac{(\nu+1)(\nu+2)}{2z^2}+\frac{(\nu+1)(\nu+2)(\nu+3)(\nu+4)}{8z^4}+\cdots\right).\end{aligned}$$

Each of these terms has an unavoidable error since the series is only asymptotically correct. If ϕ is zero, Eq. (A4) applies—which is just the first term of the above expansion—and the second term is smaller than the unavoidable error in the first term so that it should not be included. However, if ϕ is equal to π, the roles are exchanged: the first term is now smaller than the unavoidable error in the second term and should not be included. This phenomenon is known as the Stokes' phenomenon.[24] Therefore, for the limit as $|z|\rightarrow\infty$ the parabolic cylinder functions behave as

$$\begin{aligned}D_\nu(|z|)&\approx e^{-(1/4)z^2}|z|^\nu,\\D_\nu(-|z|)&\approx\frac{\sqrt{2\pi}}{\Gamma(-\nu)}e^{(1/4)z^2}|z|^{-\nu-1}.\end{aligned} \tag{A5}$$

The asymptotic expansions of the parabolic cylinder functions (A5) prove useful to evaluate the Wronskian,

$$\begin{aligned}D_\nu(z)\partial_z D_\nu(-z)-D_\nu(-z)\partial_z D_\nu(z)&\rightarrow\frac{1}{z}\frac{\sqrt{2\pi}}{\Gamma(-\nu)}\\&\times\left(z-\frac{\nu+1}{z}-\frac{\nu}{2}\right)\rightarrow\frac{\sqrt{2\pi}}{\Gamma(-\nu)}=W,\end{aligned} \tag{A6}$$

as well as to calculate the parabolic cylinder functions for large arguments numerically.

[1] S. Datta, *Electronic Transport in Mesoscopic Systems*, Cambridge Studies in Semiconductor Physics and Microelectronic Engineering Vol. 3 (Cambridge University Press, Cambridge, 1995).
[2] L. Eaves, F. W. Sheard, and G. A. Toombs, *Physics of Quantum Electron Devices*, Springer Series in Electronics and Photonics Vol. 28 (Springer-Verlag, Berlin, 1990), p. 106.
[3] D. Weiss, K. von Klitzing, K. Ploog, and G. Weimann, Europhys. Lett. **8**, 179 (1989).
[4] M. L. Roukes *et al.*, Phys. Rev. Lett. **59**, 3011 (1987).
[5] H. A. Carmona *et al.*, Phys. Rev. Lett. **74**, 3009 (1995).
[6] H. A. Carmona *et al.*, Solid-State Electron. **40**, 217 (1996).
[7] P. D. Ye, D. Weiss, R. R. Gerhardts, and H. Nickel, J. Appl. Phys. **81**, 5444 (1997).
[8] J. E. Müller, Phys. Rev. Lett. **68**, 385 (1992).
[9] F. M. Peeters and A. Matulis, Phys. Rev. B **48**, 15 166 (1993).
[10] M. Calvo, Phys. Rev. B **51**, 1168 (1995).
[11] F. M. Peeters and P. Vasilopoulos, Phys. Rev. B **47**, 1466 (1993).
[12] C. Caroli, R. Combescot, P. Nozières, and D. Saint-James, J. Phys. C **5**, 21 (1972).
[13] T. E. Feuchtwang, Phys. Rev. B **13**, 517 (1976).
[14] P. Guèret, A. Baratoff, and E. Marclay, Europhys. Lett. **3**, 367 (1987).
[15] V. M. Ramaglia, A. Tagliacosso, F. Ventriglia, and G. P. Zucchelli, Phys. Rev. B **43**, 2201 (1991).
[16] C. Heide and N. F. Schwabe, Phys. Rev. B **57**, 11 862 (1998).
[17] Y. Meir and N. S. Wingreen, Phys. Rev. Lett. **68**, 2512 (1992).
[18] P. A. Crowell *et al.*, J. Appl. Phys. **81**, 5441 (1997).
[19] F. M. Peeters and P. Vasilopoulos, Phys. Rev. B **47**, 1466 (1993).
[20] V. M. Ramaglia and F. Ventriglia, J. Phys. C **3**, 4881 (1991).
[21] J. H. Davies and A. Larkin, Phys. Rev. B **49**, 4800 (1994).
[22] N. S. Wingreen, K. W. Jacobsen, and J. W. Wilkins, Phys. Rev. B **40**, 11 834 (1989).
[23] W. Magnus, F. Oberhettinger, and R. P. Soni, *Formulas and Theorems for Special Functions of Mathematical Physics* (Springer-Verlag, New York, 1966).
[24] P. M. Morse and H. Feshbach, *Methods of Theoretical Physics* (McGraw-Hill Book Company, New York, 1953).